RSC Advances

PAPER

View Article Online
View Journal | View Issue

Cite this: *RSC Adv.*, 2020, **10**, 36971

Dansyl-modified carbon dots with dual-emission for pH sensing, Fe^{3+} ion detection and fluorescent ink

Hua Tian,[a] Yongcheng Dai,[a] Wenzhe Fu,[a] Haifang Liu,[b] Mengting Li,*[a] Meiyuan Lv[a] and Xueqiong Yin *[a]

Received 13th July 2020
Accepted 24th August 2020

DOI: 10.1039/d0ra06097f

rsc.li/rsc-advances

In this work, a multifunctional ratiometric fluorescence (FL) nanohybrid (CSCDs@DC) was synthesized from chitosan based carbon dots (CSCDs) and dansyl chloride (DC) at room temperature. The CSCDs@DC revealed strong FL intensity, great stability and excellent anti-photobleaching properties. Herein, CSCDs@DC was responsive to pH value in the range of 1.5–4.0 and exhibited color-switchable FL properties between acidic and alkaline environments. In addition, CSCDs@DC showed good selectivity and sensitivity towards Fe^{3+} ions. A good linear relationship for the Fe^{3+} ion detection was obtained in the range from 0 μM to 100 μM, with a detection limit of 1.23 μM. What's more, CSCDs@DC can be used as a fluorescent ink. It expressed superior optical properties after 3 months of storage or continuous exposure to UV light for 24 h. This study suggested that CSCDs@DC had potential in the detection of pH and metal ions, as well as showing promising application in the anti-counterfeiting field.

Introduction

As we all know, pH and metal ions play important roles in the environment, and biological and industrial areas, and both have received great research interest in the past decade.[1,2] Monitoring the change of pH value is needed due to its great impact.[3] In the environment field, acid rain and raw sewage result in the pollution of soil and water, which is attributed to the change of pH values.[4] Besides, in the biological area, pH has a close relationship with active compounds in biological macromolecules.[5] Therefore, it is very important to measure the pH variation in our surroundings. Nowadays, there are many methods and techniques for pH sensing. In particular, optical method has attracted a lot of attention in pH measurement attribute to the good performance of rapid response, high signal-to-noise ratio, and good sensitivity.[6] Metal ions play the crucial roles in the metabolism.[7] Deficiency of Fe^{3+} ions in the body may decrease oxygen delivery to cells, which would lead to anemia. While excess Fe^{3+} ions in a living cell can cause serious damage such as liver and kidney diseases.[8] Moreover, Fe^{3+} ion has an important effect on the environment. Indirectly, low concentration iron in high nutrient low chlorophyll areas became the limitation for primary productivity (algal growth) in vast areas of the oceans, which might result in the regulation of the global climate *via* a reduction of the ability of the oceanic phytoplankton to sink atmospheric CO_2.[9] Therefore, it is very important to quantify Fe^{3+} ions content. To date, many approaches have been utilized to evaluate the presence of Fe^{3+} ions, such as inductively coupled plasma mass spectrometry, atomic absorption spectrometry, spectrophotometry, and voltammetry.[10–13] However, these methods are either time-consuming, expensive equipment requirement or tedious sample pretreatment. Therefore, it is necessary to find a rapid and accurate method to detect Fe^{3+} ions. Acid rain is an important environmental pollutant, whose pH can reach 1.5–4.5.[14] Acidic water with a pH of approximately 5.2 or even lower can promote the corrosion of metal surfaces. pH can change the solubility of heavy metals from construction and demolition waste, and most heavy metals exist a secondary dissolution at pH 5.3. Under lower pH condition, the desorption of metals such as Fe will be increased significantly.[15] Fe^{3+} ions released from buildings or industrial wastes caused by acid rain has caused serious environmental and health problems. Therefore, the pH value and Fe^{3+} ions content in acid rain need to be monitored simultaneously. It would be interesting to develop a multi-mode platform to address the issues by an all-in-one strategy.

Recently, the fluorometric detection methods have been applied in visualization inspections due to high sensitivity, good selectivity and rapid response. Fluorescent carbon dots (CDs) have been revealed to be a promising fluorescent material because of the outstanding properties, such as good

[a]*Hainan Provincial Fine Chemical Engineering Research Center, School of Chemical Engineering and Technology, Hainan University, 58th Renmin Road, Haikou, Hainan, 570228, P. R. China. E-mail: limengting2016@163.com; yxq88@hotmail.com; Fax: +86 898 66291383; Tel: +86 898 66279161; +86 13138907588*

[b]*Central Laboratory, Affiliated Haikou Hospital Xiangya School of Medicine, Central South University (Haikou Municipal People Hospital), Haikou, Hainan 570208, P. R. China*

fluorescence (FL) stability, strong water solubility, biocompatibility, low toxicity, abundant precursor sources and facile functionalization property.[16–18] Besides, doping is an effective approach to improve the optical properties. For example, B, N, S, and P could improve emission properties of CDs. Among these, N-doping was very effective.[19] The amino functional groups on the surface of CDs can improve the water solubility, reduce the potential biotoxicity and enhance the photoluminescence property.[20,21] Thus, N-doped CDs had been prepared by various methods and widely applied in sensing. Chitosan (CS) is a natural copolymer, which is obtained by deacetylation of chitin. CS contains the monomers of 2-aminoglucose and *N*-acetylaminoglucose,[22] which makes it an interesting precursor for N-doped CDs preparation. Janus *et al.* synthesized N-doped chitosan-based CDs with high quantum yield (11.5%) in a microwave radiation field. The CDs had nontoxicity and could be a potential in biomedical applications.[23] In summary, CS is a good raw material for N-doped CDs that have good water solubility, photoluminescence property and low toxicity.

There are a few reports about N-doped CDs fluorescent methods for pH and Fe^{3+} ions sensing. Wang *et al.* synthesized N-doped CDs by hydrothermal carbonization. The N-doped CDs displayed a remarkable emission enhancement when the pH was increased from 2 to 10. And it showed a good linear relationship when the concentration of Fe^{3+} is in the range from 0 to 1.6 μM.[24] Chen *et al.* reported that N-CDs showed strong orange fluorescence, certain water solubility property and obvious FL quenching to Fe^{3+} ions and pH. Furthermore, the N-CDs exhibited outstanding biocompatibility and cell imaging ability. The N-CDs were successfully introduced into HeLa cells to detect intracellular Fe^{3+}.[25] Nevertheless, most of these fluorescent sensors depend on a single emission intensity change, which can be affected by many factors including instrumental efficiency, environmental conditions and the concentration of probe molecules. Thus, ratiometric fluorescent sensors which can produce dual-emission fluorescence were developed. Compared with the single-emission fluorescent response, the ratiometric fluorescent sensor can eliminate the described disadvantages and make the detection become more sensitive and accurate.[26] In addition, the ratiometric fluorescent sensor can offer a built-in environmental interference correction, which excludes the fluctuation of light excitation intensity.[27] With these in mind, many CDs have been synthesized and constructed as ratiometric FL sensors for pH, thiols, heavy-metal. Sun *et al.* synthesized multicolor emissive carbon dots as a ratiometric fluorescent sensor for Fe^{3+} ions detection by microwave irradiation.[28] Xia *et al.* developed a kind of intrinsic dual-emission CDs *via* a facile hydrothermal for ratiometric fluorescent pH sensing.[29] However, few CDs based ratiometric fluorescent sensors are used for pH sensing and Fe^{3+} ions detection simultaneously. Therefore, it is significant to design a multifunctional ratiometric fluorescent sensor with CDs for both evaluations directly.

Dansyl (1-(dimethylamino)-naphthalene-5-sulfonyl) fluorophore has attractive properties due to its intense absorption bands in the near UV and a strong FL in the visible region with high emission quantum yields and easy derivation.[30] In addition, dansyl fluorophore is sensitive to micro-environmental change attributed to intramolecular charge transfer (ICT) and easy to be introduced at the N-terminal of many compounds containing amino group.[31–35] These characteristics make dansyl fluorophore a core structure in most fluorescent sensors for detecting anions and cations.[36] There are some reports on the synthesis of FL sensors by grafting dansyl fluorophore with organic compounds, but such sensors need detect targets in organic reagents. For example, Chen *et al.* synthesized a fluoride selective fluorescent chemosensor based on sulfonamide derivatives for fluoride ion detection in acetonitrile.[37] Liu *et al.* prepared a fluorescent sensor containing hydrazide and dansyl groups for amino acid anions recognition in $CHCl_3$.[38] Originally, dansyl chloride (DC) can't dissolve in water, which limits

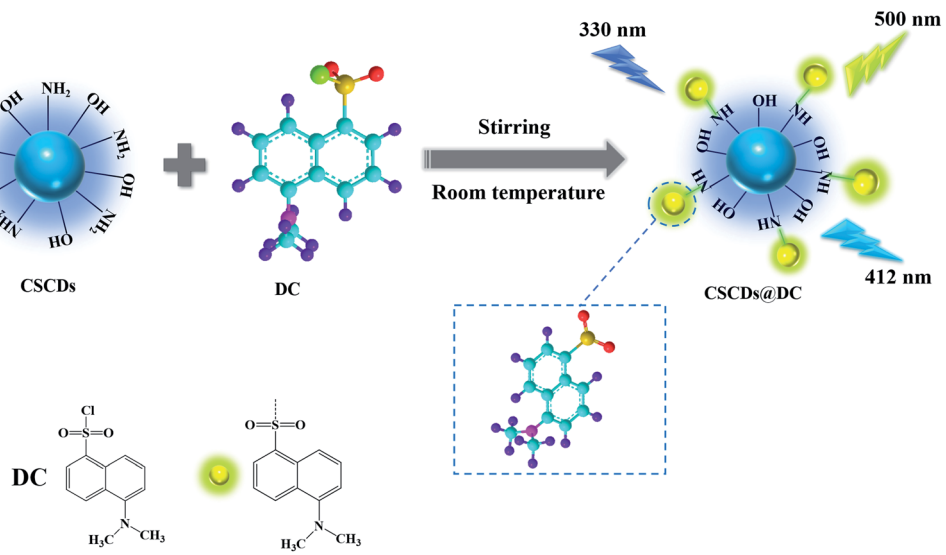

Scheme 1 Illustration for the preparation of CSCDs@DC.

its application. While, we found that the solubility can be improved by grafting the dansyl fluorophore onto CDs through the amino group. Furthermore, by combining dansyl fluorophore and amino groups, sulfonyl groups can be converted into sulfonamide groups with stronger electron absorption ability, which is beneficial to ICT fluorescence emission.

In this study, we designed a multifunctional ratiometric FL nanohybrid (CSCDs@DC) by grafting dansyl fluorophore onto N-doped CDs (CSCDs), which can be employed as sensor in the pH sensing and Fe^{3+} ions detection. Furthermore, CSCDs@DC was also investigated as fluorescent inks. CSCDs@DC showed good selectivity, high sensitivity and great stability. The CSCDs were prepared by hydrothermal treatment of CS. CSCDs@DC was fabricated by modifying the CSCDs with dansyl fluorophore at room temperature (Scheme 1). The chemical structure and optical properties of CSCDs@DC were characterized by the transmission electron microscopy (TEM), the Fourier transform infrared spectroscopy (FTIR), the UV-vis spectrophotometry and the FL spectrophotometry. Our study provided a new strategy for developing the multifunctional fluorescence platform based on carbon dots.

Experimental

Materials

Chitosan (CS, deacetylation degree $\geq$ 95%, Aladdin Ltd.), dansyl chloride (DC, Sigma-Aldrich). All other reagents used in the experiment were analytical grade and used without further purification. Ultrapure water was used throughout the experiment. $FeCl_3$, $CaCl_2$, $FeSO_4 \cdot 7H_2O$, $CdN_2O_6 \cdot 4H_2O$, $Mg(NO_3)_2 \cdot 6H_2O$, $Cu(NO_3)_2 \cdot 4H_2O$, $BaCl_2 \cdot 2H_2O$, $HgCl_2$, $K_2Cr_2O_7$, $Pb(NO_3)_2$ were purchased from Guangzhou Chemical Reagent Factory (Guangzhou, China). Stock solutions of CSCDs@DC (1.0 mg mL^{-1}) were prepared in the ultrapure water.

Preparation of CSCDs

CSCDs were prepared according literature and modified accordingly.[20] 1 g CS was dispersed in 20 mL ultrapure water by stirring with a magnetic stirrer at room temperature. Then the mixture solution was transferred to a poly(tetrafluoroethylene) (Teflon)-lined autoclave and heated at 160 °C for 12 h. After the reaction, the reactor was cooled down to room temperature naturally. The brown-yellow product was centrifuged at 8000 rpm for 20 min and passed through a 0.22 μm micron filter.

Synthesis of CSCDs@DC

The CSCDs@DC was prepared through a facile method. DC was dissolved in acetone and then added into CSCDs solution. The reaction mixture was stirred for 12 h at room temperature and further removed the acetone by applying vacuum-rotary evaporation. Then the mixture was centrifuged at 8000 rpm for 10 min and passed through a 0.22 μm micron filter. Finally, the suspension was dialyzed against ultrapure water through a dialysis membrane (MWCO 500–1000 Da) for 24 h and then freeze dried. The CSCDs@DC was dispersed in the ultrapure water as stock solution (1 mg mL^{-1}) for further study. The synthetic mechanism for the preparation of the CSCDs@DC was shown in Scheme 1.

Detection of pH

1 M HCl solution, 1 M NaOH solution and 0.1 M phosphate buffer solution (PBS) were prepared and mixed with different volume ratio to get solutions with different pH value (1.0, 1.5, 2.0, 2.5, 3.0, 3.5, 4.0, 5.0, 6.0, 7.0, 8.0, 9.0, 10.0, 11.0, 12.0). Then, 300 μL CSCDs@DC and 1.7 mL solution with different pH value were pipetted into 4 mL cuvette. The FL intensity was then measured with excitation at 330 nm. The relationship between FL intensity and the pH value was studied.

Detection of Fe^{3+} ions

The selectivity of CSCDs@DC as a sensor for the detection of Fe^{3+} ions was explored. The different metal ions including Ba^{2+}, Ca^{2+}, Cd^{2+}, Cu^{2+}, Fe^{2+}, Fe^{3+}, Hg^{2+}, Mg^{2+}, Pb^{2+}, $Cr_2O_7^{2-}$ at a concentration of 100 μM were mixed with 0.4 mg mL^{-1} CSCDs@DC aqueous solution, respectively.[39] The effect of typical interfering metal ions on the FL behavior of CSCDs@DC was investigated to evaluate the selectivity of CSCDs@DC. The sensitivity of Fe^{3+} ions detection was performed by adding different concentrations of Fe^{3+} ions at room temperature. The pH of the mixed solution was adjusted to 6.0. The FL intensity was measured with excitation at 330 nm.

Instrumentation

The transmission electron microscopic (TEM) image was performed on a JEM-2100 microscope using an acceleration voltage of 200 kV. Fourier transform infrared spectroscopy (FTIR) experiments were conducted on a Bruker TENSOR 27 spectrometer in the form of KBr pellets. The UV-vis absorption spectra were recorded on a TU-1901 UV-vis spectrophotometer (China). FL emission spectra were recorded by a F-320 fluorescence spectrophotometer (China).

Results and discussion

Optimization of synthesis conditions of CSCDs@DC

To investigate the optical properties of CSCDs, DC and CSCDs@DC, the absorbance and FL spectra were performed. In Fig. 1a, compared the FL spectra of CSCDs, DC and CSCDs@DC, the FL emission of CSCDs was at 412 nm, however, the FL emission of DC was not observed. Furthermore, the FL emission spectra of CSCDs@DC in aqueous solution showed the marked dual emission peak positions at 412 nm and 500 nm under an excitation of 330 nm. The solvatochromic effect of the FL spectra of CSCDs@DC was determined. Fig. 1b shows that CSCDs@DC exhibited a red-shift of 26 nm, when the solvent polarity was increased gradually from DMF to H_2O: 474 nm in DMF, 485 nm in CH_3CN, 500 nm in H_2O. The FL intensity of CSCDs@DC exhibited an obvious decreasing with increasing solvent polarity. The results of solvatochromic effect indicated a charge-transfer (CT) state.[40,41] It was considered that the sharp

FL intensity of CSCDs@DC at 500 nm was ascribed to ICT.[34,42] It indicated the formation of fluorescent CSCDs@DC.

To establish the ratiometric fluorescent assay, the mass ratio of CSCDs and DC was investigated in detail. As shown in Fig. 1c, the ratio of the two fluorescent components had a significant effect on the FL intensities of the sensor. The fluorescent CSCDs@DC with different mass ratio had emissions at 412 nm and 500 nm under an excitation of 330 nm. When the CSCDs/DC ratio changed from 1 : 2 to 40 : 1, F_{412}/F_{500} changed visibly. Firstly, when DC mass increasing, the amount of dansyl group grafted onto the CSCD increased. Therefore, the FL intensity at 500 nm increased. When the CSCDs/DC ratio was 20 : 1, F_{412} and F_{500} became nearer, suggesting a more flexible scope of ratiometric variation.[43] By contrast, when the CSCDs/DC ratio deviated from this value, a negligible peak at 412 nm or 500 nm was observed. It was probably that too much CSCDs or dansyl fluorophore could submerge the FL from each other. Thus, a suitable ratio of 20 : 1 was adopted in the following study.

Optical properties

The UV-vis spectra are shown in Fig. 1d. The three absorption peaks at 210 nm, 242 nm and 310 nm were ascribed to the π–π* transition of the C=C bond, the π–π* transition of aromatic sp^2 hybridization, and n–π* transition of the C=O bond,[44,45] respectively. CSCDs (red) had two absorption peaks at 210 nm and 310 nm. CSCDs@DC (black) had three absorption peaks at 210 nm, 242 nm and 310 nm. The absorption peaks at 242 nm attributed to the π–π* transition of aromatic sp^2 hybridization. It indicated dansyl fluorophores were introduced onto CSCDs. In addition, the effect of ionic strength on the FL stability of CSCDs@DC was investigated. As shown in Fig. 1e, F_{412} (red) and F_{500} (green) of CSCDs@DC did not change obviously under various concentrations of NaCl, which revealed that CSCDs@DC was stable in the salt environments.

Structural features of CSCDs@DC

Fig. 2a and b show the TEM images of CSCDs and CSCDs@DC with a scale bar of 20 nm. Fig. 2a expresses the spherical shaped CSCDs particles are uniformly dispersed without apparent aggregation. The particle size distribution of CSCDs was calculated by Nano Measurer. The diameter of CSCDs is mainly distributed in the range of 1.5–6.8 nm, with the mean diameter of 3.6 nm. As shown in Fig. 2b, it was observed that CSCDs were covered by DC. And larger particles were formed apparently in the TEM image of CSCDs@DC. It indicates the formation of the CSCDs@DC nanohybrid.

The FTIR spectra are shown in Fig. 2c. The peaks at 3600–3200 cm^{-1} were attributed to the stretching vibrations of O–H and N–H.[46] The FTIR spectrum of CSCDs (the blue curve) indicated that the absorption band 1600 cm^{-1} was the bending vibrations of amine group (–NH_2).[47] The absorption band at 1385 cm^{-1} was associated with C–H and N–H bending vibrations.[48] The peak at 1077 cm^{-1} was ascribed to the stretching of the C–O,[49] and the peak at 826 cm^{-1} was N–H deformation vibration.[6] These peaks suggested that the function groups (–NH_2, –OH) existed on the surface of CSCDs. In the spectrum of DC (the red curve), the peak at 1148–1252 cm^{-1} was

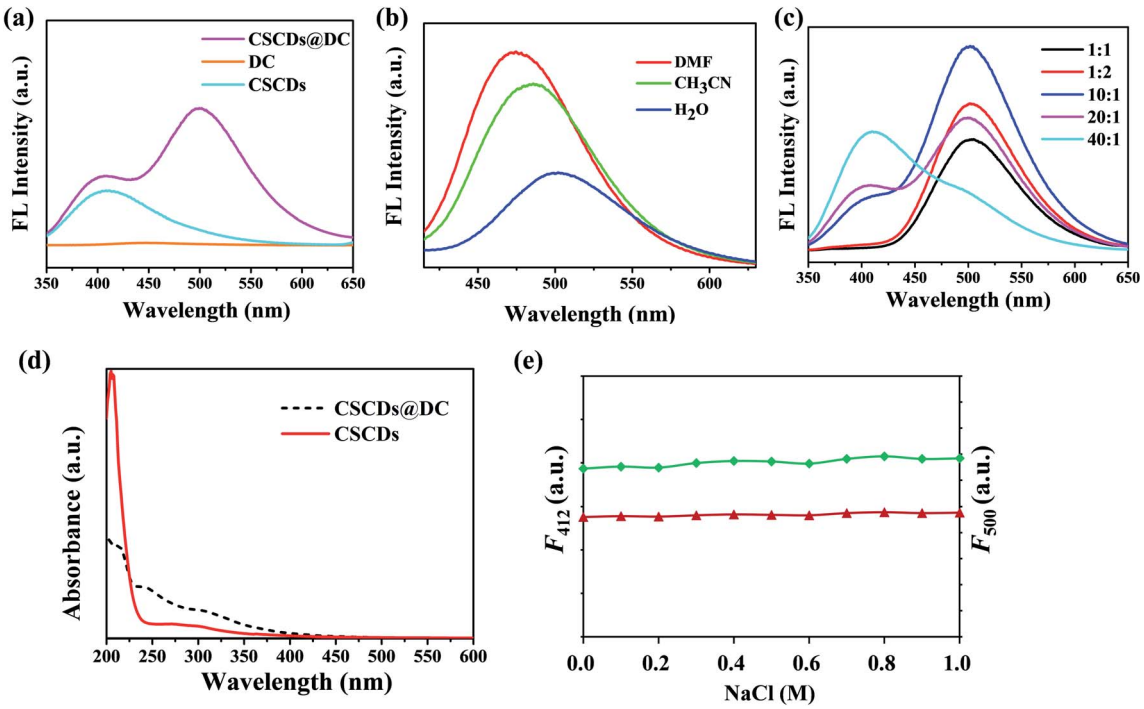

Fig. 1 (a) FL emission spectra of CSCDs@DC, DC and CSCDs. (b) FL spectra of CSCDs@DC in different solvents. (c) Effect of CSCDs/DC mass ratio on the FL intensity at 412 nm and 500 nm. (d) UV-vis absorption spectra of CSCDs@DC and CSCDs. (e) F_{412} (red) and F_{500} (green) with ion strength.

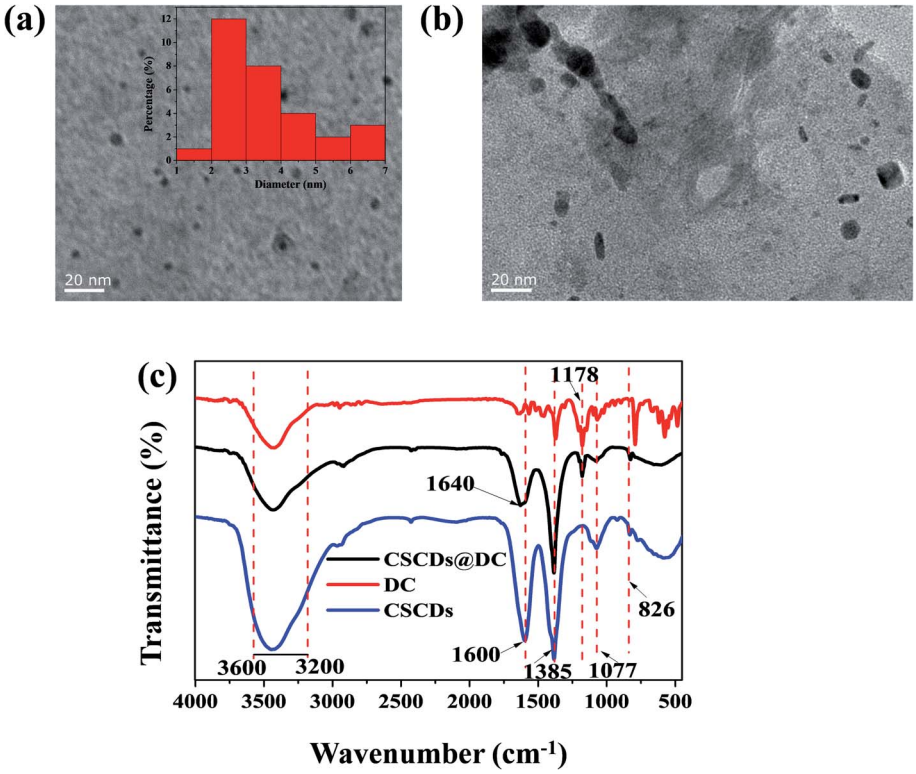

Fig. 2 (a) TEM image of CSCDs (the inset is the particle size distribution histogram). (b) TEM image of CSCDs@DC. (c) The FTIR spectra of CSCDs, DC and CSCDs@DC.

corresponded to O═S═O asymmetric stretch indicated the presence of sulfamate groups.[50] Compared with the FTIR spectra of CSCDs and DC, there were the characteristic peaks of $-NH_2$, N–H, –OH, and O═S═O in CSCDs@DC (the black curve). The absorption intensity at 1600 cm^{-1} in the spectrum of CSCDs@DC was obviously weaker than in that of CSCDs. And it was found that there was a new peak at 1640 cm^{-1} which was ascribed to the amide bond.[51] It indicated the sulfonyl group in the dansyl fluorophore converted into sulfonamide. These results revealed that the dansyl fluorophores had connected to

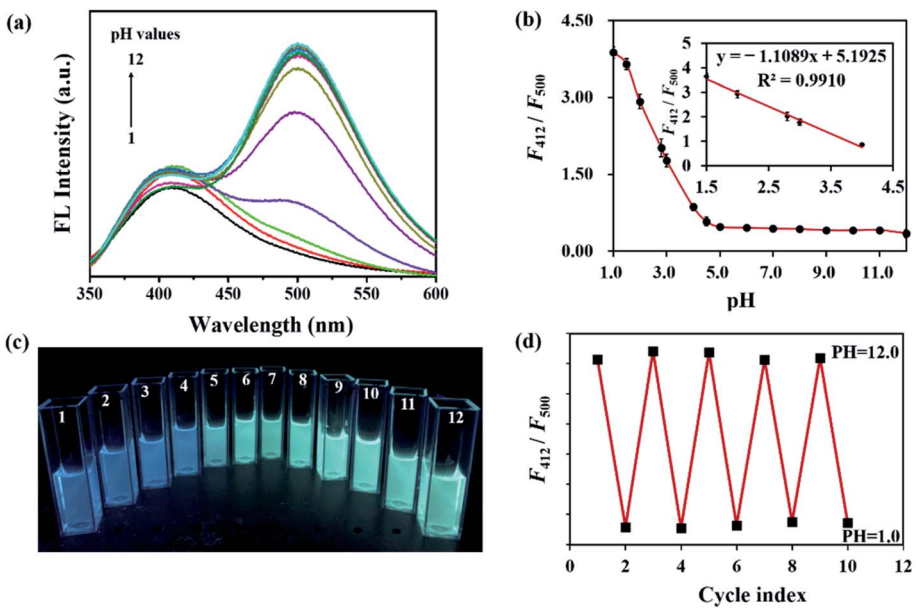

Fig. 3 (a) FL spectra of CSCDs@DC at different pH values. (b) Influence of pH values on the FL intensity (F_{412}/F_{500}) of CSCDs@DC. Inset is linear relationship of the ratiometric FL intensity (F_{412}/F_{500}) *versus* pH values. (c) Photo of CSCDs@DC aqueous solution with different pH values (1–12) irradiated by 365 nm UV light. (d) FL reversibility against pH change between 1.0 and 12.0, repeatedly.

the amino groups on the surface of CSCDs. The characterization proved that the CSCDs@DC was synthesized using a facile method.

pH-response property

In Fig. 3a, the effect of pH on the FL behavior of CSCDs@DC was explored by changing the pH values from 1.0 to 12.0. In the pH-response assay, the FL intensity of CSCDs@DC emission at 412 nm was basically stable. However, the FL intensity at 500 nm exhibited a decrease in acid solutions, whereas almost no change was observed in neutral to alkaline solutions. As shown in Fig. 3b, the ratiometric FL intensity (F_{412}/F_{500}) of CSCDs@DC decreased at different pH values from 1.0 to 4.0, while changed negligibly at the pH values from 5.0 to 12.0. Meanwhile, the inset in Fig. 3b showed a good linear relationship of F_{412}/F_{500} against pH value in the range of 1.5–4.0, (regression equation: $y = -1.1089x + 5.1925$, $R^2 = 0.9910$). Compared with the reported CDs[52] which displayed a good linear relationship in the range of 4.0 to 6.5, the CSCDs@DC could accurately test the pH value of strong acidic solutions (pH 1.5–4.0). Given such property, the CSCDs@DC could be used as a new kind of pH sensor.

Fig. 3c shows a gradient color change of CSCDs@DC solution with different pH values from 1.0 to 12.0 irradiated by 365 nm UV light. It exhibited blue color in acidic solution (pH ≤ 4) and green color in basic solution. It also indicated that F_{412} was not affected by pH, and F_{500} had a quenching in an acidic environment. The quenching of FL intensity at 500 nm might be due to the reduction of ICT by the protonation of dimethylamine at lower pH values.[51,53] Therefore, F_{500} could be used as the testing signal while F_{412} as the internal standard signal in pH measurements. In addition, the FL reversibility against pH was carried out by adjusting the pH values between 1.0 and 12.0 repeatedly. As shown in Fig. 3d, the ratiometric FL intensity (F_{412}/F_{500}) of CSCDs@DC presented a good reproducibility between the strong acidic solution (pH 1.0) and the strong alkaline solution (pH 12.0). CSCDs@DC exhibited good photostability and FL reversibility in different pH solutions. Thus, it can be applied as an excellent nanosensor for environment and industry pH measurement.

Sensing of Fe^{3+} ions

As shown in Fig. 4a, F_{500} under an excitation of 330 nm was more decreased in the presence of Fe^{3+} ions than other metal ions (Ba^{2+}, Ca^{2+}, Cd^{2+}, Cu^{2+}, Fe^{2+}, Fe^{3+}, Hg^{2+}, Mg^{2+}, Pb^{2+}, $Cr_2O_7^{2-}$), and F_{412} changed less noticeably than F_{500}. Therefore, F_{412}/F_{500} was used to indicate the change of FL. Only Fe^{3+} ions induced a distinct change of F_{412}/F_{500}, whereas other metal ions caused almost no change. Meanwhile, the influence of interference on sensing of Fe^{3+} ions was evaluated by adding Fe^{3+}

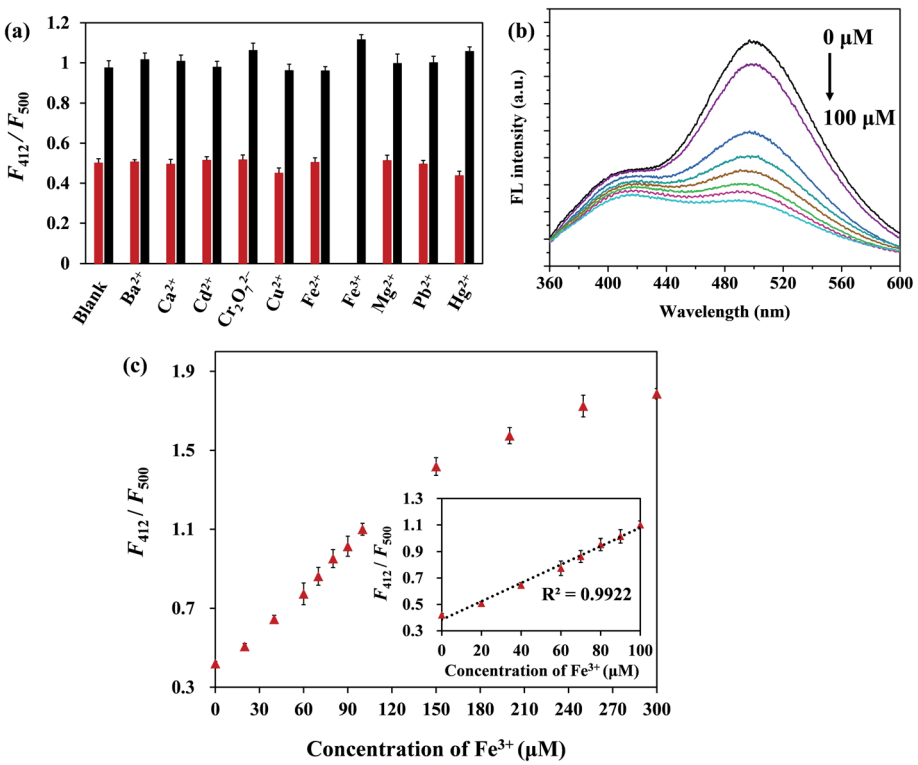

Fig. 4 (a) Selectivity of CSCDs@DC (0.4 mg mL^{-1}) aqueous solution for Fe^{3+} ions over other metal ions. The red bars represented the addition of metal ions (100 μM for all the metal ions). The black bars represented the subsequent addition of 100 μM Fe^{3+} to the CSCDs@DC aqueous solution. (b) FL spectra of CSCDs@DC (0.4 mg mL^{-1}) with different concentrations of Fe^{3+} ions at 330 nm. (c) FL emission ratios (F_{412}/F_{500}) of CSCDs@DC (0.4 mg mL^{-1}) in the presence of different Fe^{3+} ions concentrations in the range from 0 μM to 300 μM. Inset is linear relationship between F_{412}/F_{500} and Fe^{3+} ions concentration in the range from 0 μM to 100 μM.

Table 1 Comparison of the performances of proposed sensor for Fe^{3+} ions

Fluorescent materials	Detection limit	Linear range	Reference
Cu-MOFs	1.56 μM	2–180 μM	60
N-CDs	32 μM	0–500 μM	61
NBCDs	7.50 μM	0–0.7 mM	62
N-CDs	0.28 μM	1–21 μM	63
BNQDs	0.3 μM	0–1 μM	64
CSCDs@DC	1.23 μM	0–100 μM	This work

ions in the presence of other metal ions. With the subsequent addition of Fe^{3+} ions into other metal ion solutions respectively, F_{412}/F_{500} was increased markedly. It revealed that the CSCDs@DC had high selectivity and good anti-interference ability for the Fe^{3+} detection.

Fig. 4b shows the FL quenching of CSCDs@DC at various concentrations of Fe^{3+} ions. The FL emission ratio (F_{412}/F_{500}) increased progressively with increasing the concentrations of Fe^{3+} ions, which indicated that the sensing system was sensitive to Fe^{3+} ions concentration. The relationship between F_{412}/F_{500} and Fe^{3+} ions concentration was presented in Fig. 4c. A good linear relationship was obtained in the range from 0 μM to 100 μM. The linear equation was $F_{412}/F_{500} = 0.0070Q + 0.3844$ ($R^2 = 0.9922$), where Q was the concentration of Fe^{3+} ion. On the basis of three times the standard deviation of 11 measurements of the blank signal of CSCDs@DC aqueous solution, the limit of detection (LOD) was 1.23 μM (LOD = $3\sigma/K$) in the range of 0–100 μM.[54,55] The LOD was much lower than the Fe^{3+} ions permissible level in drinking water (5.4 μM) proposed by the Environmental Protection Agency (EPA).[56] It was also comparable to the part previous reported proposed sensor for Fe^{3+} ions listed in Table 1. Therefore, the CSCDs@DC for the detection of Fe^{3+} ions had the superiority of wide linear ranges, low detection limit, simple operation, excellent selectivity and high sensitivity.

When Fe^{3+} ions were added to the as-prepared CSCDs@DC aqueous solution, F_{500} was obviously quenched. Upon the

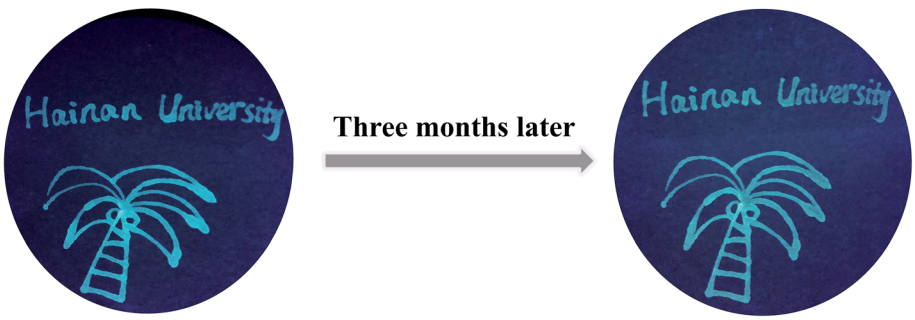

Fig. 5 Photo of painting by CSCDs@DC under the UV light.

Fig. 6 Photo of painting by CSCDs@DC after continuous UV light exposure.

addition of an increasing amount of Fe^{3+}, F_{500} gradually decreased. There were sulfonamide and hydroxy groups existed on the CSCDs@DC. It may originate from the complexation of the N in sulfonamide and the O in hydroxy group with Fe^{3+}.[57] Such complexation promoted the abundant electrons in the excited state of CSCDs@DC transferring to the 3d orbital of Fe^{3+} and finally caused the strong FL quenching. Meanwhile, the Fe^{3+}-centered d–d states placed below the fluorophore π–π* states and can be used to deactive the fluorophore by electron transfer.[58,59] Therefore, the ICT between CSCDs and dansyl group was blocked, then F_{500} was visibly reduced.

Application in fluorescent ink

The strong FL intensity and great stability could also make CSCDs@DC become a potential alternative of the existing fluorescent inks. The CSCDs@DC aqueous solution was used to write on a filter paper. As shown in Fig. 5, the filter paper under 365 nm UV light showed a bright green FL and a clear pattern shape. After keeping for three months at room temperature and ambient pressure, the pattern still emitted a clear and intense green light under 365 nm UV excitation. It showed more excellent FL stability compared with the report that the CDs still had blue fluorescent characters after keeping a month.[65] Furthermore, in Fig. 6, the hand-written patterns were still clearly visible after continuous exposure of UV light for 24 h. The results showed that the CSCDs@DC displayed strong resistance to photobleaching. Zhao *et al.* studied the FL stability and anti-photobleaching by irradiating GQD ink printed images under UV light for 180 min.[66] In comparison to this report, our CDs ink hand-written patterns were more stable because the patterns can still be seen clearly in 24 h UV illumination. It indicates the CSCDs@DC ink is satisfactorily stable and retains the FL property for a long time.[67] Herein, this study proved that the CSCDs@DC can be used as an alternative of fluorescent ink in anti-counterfeiting, information storage and information encryption fields.

Conclusions

A new multifunctional ratiometric fluorescent nanohybrid called CSCDs@DC was synthesized from DC and CSCDs by a simple method at room temperature. The characterization of UV, FL, FTIR and TEM indicated that DC reacted with CSCDs by incorporating the dansyl group onto the surface of CSCDs. CSCDs@DC showed dual emission peaks at 412 nm and 500 nm. The FL intensity at 500 nm could respond to pH values and Fe^{3+} ions, while the FL intensity at 412 nm remained constant. The FL intensity of CSCDs@DC was pH dependent and performed a good linear relationship in the pH range of 1.5–4.0. In addition, CSCDs@DC enabled convenient detection of Fe^{3+} ions with a low LOD (1.23 μM). Importantly, the detection of pH values and Fe^{3+} ions content was executed simultaneously by both visible and FL variation. Moreover, the CSCDs@DC aqueous solution written on a filter paper expressed excellent FL stability and anti-photobleaching. The study indicated that the CSCDs@DC could be a kind of promising material used in environmental, biological, anti-counterfeit applications and so on.

Conflicts of interest

There are no conflicts to declare.

Acknowledgements

This work was financially supported by the Key Research and Development Project of Hainan Province (ZDYF2018232), the Project of Scientific Research Platform Construction of Hainan University (ZY2019HN09) and the National Science Foundation of China (21466011).

References

1 H. Ehtesabi, Z. Hallaji, S. Najafi Nobar and Z. Bagheri, *Microchim. Acta*, 2020, **187**, 150.
2 S. Chowdhury, M. A. J. Mazumder, O. Al-Attas and T. Husain, *Sci. Total Environ.*, 2016, **569–570**, 476–488.
3 C. Zhang, Y. Cui, L. Song, X. Liu and Z. Hu, *Talanta*, 2016, **150**, 54–60.
4 Y. Z. Fan, J. X. Dong, Y. Zhang, N. Li, S. G. Liu, S. Geng, Y. Ling, H. Q. Luo and N. B. Li, *Spectrochim. Acta, Part A*, 2019, **219**, 382–390.
5 J. H. Yoon, S. B. Hong, S. O. Yun, S. J. Lee, T. J. Lee, K. G. Lee and B. G. Choi, *J. Colloid Interface Sci.*, 2017, **490**, 53–58.
6 J. Shangguan, D. He, X. He, K. Wang, F. Xu, J. Liu, J. Tang, X. Yang and J. Huang, *Anal. Chem.*, 2016, **88**, 7837–7843.
7 M. Lan, S. Zhao, X. Wei, K. Zhang, Z. Zhang, S. Wu, P. Wang and W. Zhang, *Dyes Pigm.*, 2019, **170**, 107574.
8 J. L. Bricks, A. Kovalchuk, C. Trieflinger, M. Nofz, M. Büschel, A. I. Tolmachev, J. Daub and K. Rurack, *J. Am. Chem. Soc.*, 2005, **127**, 13522–13529.
9 S. Caprara, L. M. Laglera and D. Monticelli, *Anal. Chem.*, 2015, **87**, 6357–6363.
10 A. Molkenova, Y. Amangeldinova, D. Aben, S. Sayatova and T. S. Atabaev, *Sensing and Bio-Sensing Research*, 2019, **23**, 100271.
11 Z.-Q. Liang, C.-X. Wang, J.-X. Yang, H.-W. Gao, Y.-P. Tian, X.-T. Tao and M.-H. Jiang, *New J. Chem.*, 2007, **31**, 906–910.
12 M. Zheng and Z. Xie, *Mater. Today Chem.*, 2019, **13**, 121–127.
13 C. M. G. van den Berg, *Anal. Chem.*, 2006, **78**, 156–163.
14 A. M. Agrawal, *J. Environ. Biol.*, 2008, **29**, 15–24.
15 B. Zhao, A. Liu, G. Wu, D. Li and Y. Guan, *J. Environ. Sci.*, 2017, **51**, 284–293.
16 W. Gao, Y. Zhou, C. Xu, M. Guo, Z. Qi, X. Peng and B. Gao, *Sens. Actuators, B*, 2020, **147**, 453–462.
17 W. Gao, Y. Ma, Y. Zhou, H. Song, L. Li, S. Liu, X. Liu, B. Gao, C. Liu and K. Zhang, *Mater. Lett.*, 2018, **216**, 84–87.
18 H. Song, Y. Zhou, C. Xu, X. Wang, J. Zhang, Y. Wang, X. Liu, M. Guo and X. Peng, *Dyes Pigm.*, 2019, **162**, 160–167.
19 H. Wang, S. Liu, Y. Xie, J. Bi, Y. Li, Y. Song, S. Cheng, D. Li and M. Tan, *New J. Chem.*, 2018, **42**, 3729–3735.
20 Y. Yang, J. Cui, M. Zheng, C. Hu, S. Tan, Y. Xiao, Q. Yang and Y. Liu, *Chem. Commun.*, 2012, **48**, 380–382.

21 R. Zhang and W. Chen, *Biosens. Bioelectron.*, 2014, **55**, 83–90.
22 A. Ray Chowdhuri, S. Tripathy, C. Haldar, S. Roy and S. K. Sahu, *J. Mater. Chem. B*, 2015, **3**, 9122–9131.
23 L. Janus, M. Piatkowski, J. Radwan-Praglowska, D. Bogdal and D. Matysek, *Nanomaterials*, 2019, **9**, 274.
24 R. Wang, X. Wang and Y. Sun, *Sens. Actuators, B*, 2017, **241**, 73–79.
25 X. Chen, J. Bai, Y. Ma, G. Yuan, J. Mei, L. Zhang and L. Ren, *Microchem. J.*, 2019, **149**, 103981.
26 S. Pang and S. Liu, *Anal. Chim. Acta*, 2020, **1105**, 115–161.
27 C. Zou, M. F. Foda, X. Tan, K. Shao, L. Wu, Z. Lu, H. S. Bahlol and H. Han, *Anal. Chem.*, 2016, **88**, 7395–7403.
28 Z. Sun, Z. Yang, L. Zhao, Y. Zhang, Y. Li, J. Hou and L. Ding, *New J. Chem.*, 2019, **43**, 853–861.
29 C. Xia, M. Cao, J. Xia, G. Zhou, D. Jiang, D. Zhang, J. Wang and H. Li, *J. Mater. Chem. C*, 2019, **7**, 2563–2569.
30 R. Métivier, I. Leray, B. Lebeau and B. Valeur, *J. Mater. Chem.*, 2005, **15**, 2965–2973.
31 G. Fiorani, M. Selva, A. Perosa, A. Benedetti, F. Enrichi, P. Licence and T. L. Easun, *Green Chem.*, 2015, **17**, 538–550.
32 L. Ding, Y. Fang, L. Jiang, L. Gao and X. Yin, *Thin Solid Films*, 2005, **478**, 318–325.
33 L. N. Neupane, J. M. Kim, C. R. Lohani and K.-H. Lee, *J. Mater. Chem.*, 2012, **22**, 4003–4008.
34 A. J. C. Silva, J. G. Silva Jr, S. Alves Jr, J. Tonholo and A. S. Ribeiro, *J. Braz. Chem. Soc.*, 2011, **22**, 1808–1815.
35 P. Srivastava, M. Shahid and A. Misra, *Org. Biomol. Chem.*, 2011, **9**, 5051–5055.
36 X.-X. Zhao, J.-F. Zhang, W. Liu, S. Zhou, Z.-Q. Zhou, Y.-H. Xiao, G. Xi, J.-Y. Miao and B.-X. Zhao, *J. Mater. Chem. B*, 2014, **2**, 7344–7350.
37 C.-F. Chen and Q.-Y. Chen, *Tetrahedron Lett.*, 2004, **45**, 3957–3960.
38 S.-y. Liu, Y.-b. He, G.-y. Qing, K.-x. Xu and H.-j. Qin, *Tetrahedron: Asymmetry*, 2005, **16**, 1527–1534.
39 W. Liu, H. Diao, H. Chang, H. Wang, T. Li and W. Wei, *Sens. Actuators, B*, 2017, **241**, 190–198.
40 W. Li, D. Liu, F. Shen, D. Ma, Z. Wang, T. Feng, Y. Xu, B. Yang and Y. Ma, *Adv. Funct. Mater.*, 2012, **22**, 2797–2803.
41 L. Yao, S. Zhang, R. Wang, W. Li, F. Shen, B. Yang and Y. Ma, *Angew. Chem., Int. Ed.*, 2014, **53**, 2119–2123.
42 A. L. Chibac, M. Simionescu, G. Sacarescu, E. C. Buruiana and L. Sacarescu, *Eur. Polym. J.*, 2017, **95**, 82–92.
43 W. Yang, J. Ni, F. Luo, W. Weng, Q. Wei, Z. Lin and G. Chen, *Anal. Chem.*, 2017, **89**, 8384–8390.
44 P. Das, M. Bose, A. K. Das, S. Banerjee and N. C. Das, *Macromol. Symp.*, 2018, **382**, 1800077.
45 M. Tang, B. Zhu, Y. Wang, H. Wu, F. Chai, F. Qu and Z. Su, *Microchim. Acta*, 2019, **186**, 604.
46 X. Jiang, J. Huang, T. Chen, Q. Zhao, F. Xu and X. Zhang, *Int. J. Biol. Macromol.*, 2020, **153**, 412–420.
47 A. P. Praxedes, A. J. da Silva, R. C. da Silva, R. P. Lima, J. Tonholo, A. S. Ribeiro and I. N. de Oliveira, *J. Colloid Interface Sci.*, 2012, **376**, 255–261.
48 X. Yang, Y. Zhuo, S. Zhu, Y. Luo, Y. Feng and Y. Dou, *Biosens. Bioelectron.*, 2014, **60**, 292–298.
49 W. Li, S. Huang, H. Wen, Y. Luo, J. Cheng, Z. Jia, P. Han and W. Xue, *Anal. Bioanal. Chem.*, 2020, **412**, 993–1002.
50 K. R. Holme and A. S. Perlin, *Carbohydr. Res.*, 1997, **302**, 7–12.
51 X. Wang, Y. Su, H. Yang, Z. Dong and J. Ma, *Colloids Surf., A*, 2012, **402**, 88–93.
52 B. Li, H. Ma, B. Zhang, J. Qian, T. Cao, H. Feng, W. Li, Y. Dong and W. Qin, *Microchim. Acta*, 2019, **186**, 341.
53 M. Zhou, X. Wang, K. Huang, Y. Huang, S. Hu and W. Zeng, *Tetrahedron Lett.*, 2017, **58**, 991–994.
54 W. Gao, H. Song, X. Wang, X. Liu, X. Pang, Y. Zhou, B. Gao and X. Peng, *ACS Appl. Mater. Interfaces*, 2018, **10**, 1147–1154.
55 X. He, Y. Han, X. Luo, W. Yang, C. Li, W. Tang, T. Yue and Z. Li, *Food Chem.*, 2020, **320**, 126624.
56 Y. Zhang, Z. Gao, X. Yang, J. Chang, Z. Liu and K. Jiang, *RSC Adv.*, 2019, **9**, 940–949.
57 C. Sha, S. Lu, F. Lv and D. Xu, *Res. Chem. Intermed.*, 2016, **42**, 5825–5834.
58 L. Fu, J. Mei, J. Zhang, Y. Liu and F. Jiang, *Luminescence*, 2013, **28**, 602–606.
59 Z. S. Qian, J. J. Ma, X. Y. Shan, H. Feng, L. X. Shao and J. R. Chen, *Chem.–Eur. J.*, 2014, **20**, 2254–2263.
60 F. Ming, J. Hou, D. Huo, J. Zhou, M. Yang, C. Shen, S. Zhang and C. Hou, *Anal. Methods*, 2019, **11**, 4382–4389.
61 J. Ahn, Y. Song, J. E. Kwon, S. H. Lee, K. S. Park, S. Kim, J. Woo and H. Kim, *Mater. Sci. Eng., C*, 2019, **102**, 106–112.
62 L. Wang, J. S. Chung and S. H. Hur, *Dyes Pigm.*, 2019, **171**, 107752.
63 X. Zhou, G. Zhao, X. Tan, X. Qian, T. Zhang, J. Gui, L. Yang and X. Xie, *Microchim. Acta*, 2019, **186**, 67.
64 B. Huo, B. Liu, T. Chen, L. Cui, G. Xu, M. Liu and J. Liu, *Langmuir*, 2017, **33**, 10673–10678.
65 D. Xu, F. Lei, H. Chen, L. Yin, Y. Shi and J. Xie, *RSC Adv.*, 2019, **9**, 8290–8299.
66 J. Zhao, Y. Zheng, Y. Pang, J. Chen, Z. Zhang, F. Xi and P. Chen, *J. Colloid Interface Sci.*, 2020, **579**, 307–314.
67 Z. Wang, D. Chen, B. Gu, B. Gao, T. Wang, Q. Guo and G. Wang, *Spectrochim. Acta, Part A*, 2020, **227**, 117671.